Design and Simulation of Superconducting Lorentz Force Electrical Impedance Tomography (LFEIT)

Boyang Shen*, Lin Fu, Jianzhao Geng, Xiuchang Zhang, Heng Zhang, Qihuan Dong, Chao Li, Jing Li, T. A. Coombs*

Electrical Engineering Division, Department of Engineering, University of Cambridge, Cambridge CB3 0FA, U.K.

*Corresponding authors. Tel.: +44 7869688318 (B. Shen), +44 1223748315 (T. A. Coombs).

E-mail addresses: bs506@cam.ac.uk (B. Shen), lf359@cam.ac.uk (L. Fu), jg717@cam.ac.uk (J. Geng), xz326@cam.ac.uk (X. Zhang), hz301@cam.ac.uk (H. Zhang), qd210@cam.ac.uk (Q. Dong), cl644@cam.ac.uk (C. Li), jl908@cam.ac.uk (J. Li), tac1000@cam.ac.uk (T. A. Coombs).

Abstract:

Lorentz Force Electrical Impedance Tomography (LFEIT) is a hybrid diagnostic scanner with strong capability for biological imaging, particularly in cancer and haemorrhages detection. This paper presents the design and simulation of a novel combination: a superconducting magnet together with LFEIT system. Superconducting magnets can generate magnetic field with high intensity and homogeneity, which could significantly enhance the imaging performance. The modelling of superconducting magnets was carried out using Finite Element Method (FEM) package, COMSOL Multiphysics, which was based on Partial Differential Equation (PDE) model with ***H***-formulation coupling ***B***-dependent critical current density and bulk approximation. The mathematical model for LFEIT system was built based on the theory of magneto-acoustic effect. The magnetic field properties from magnet design were imported into the LFEIT model. The basic imaging of electrical signal was developed using MATLAB codes. The LFEIT model simulated two samples located in three different magnetic fields with varying magnetic strength and homogeneity.

Keywords: Superconducting magnet, High Temperature Superconductor (HTS), Halbach Array, Electrical signal, Lorentz Force Electrical Impedance Tomography (LFEIT).

1. Introduction

Lorentz Force Electrical Impedance Tomography (LFEIT), also known as Hall Effect imaging (HEI) or Magneto-Acousto-Electric Tomography (MAET), is one of the most promising hybrid portable device with burgeoning potential for cancer and internal haemorrhages detection [1-3]. In contrast to ultrasonic imaging technology's disadvantage in distinguishing soft tissues as acoustic impedance varies by less than 10% among muscle and blood, LFEIT show its powerful capability in providing information about the pathological and physiological condition of tissue because electrical impedance varies widely among soft tissue types and pathological states [4]. Other than carcinomas, tissues under conditions in hemorrhage or ischemia are able to exhibit huge difference in electrical properties because most body fluid and blood have fairly different permittivity and conductivity compared to other soft tissues [5]. Fig. 1 presents the schematic of a superconducting Lorentz Force

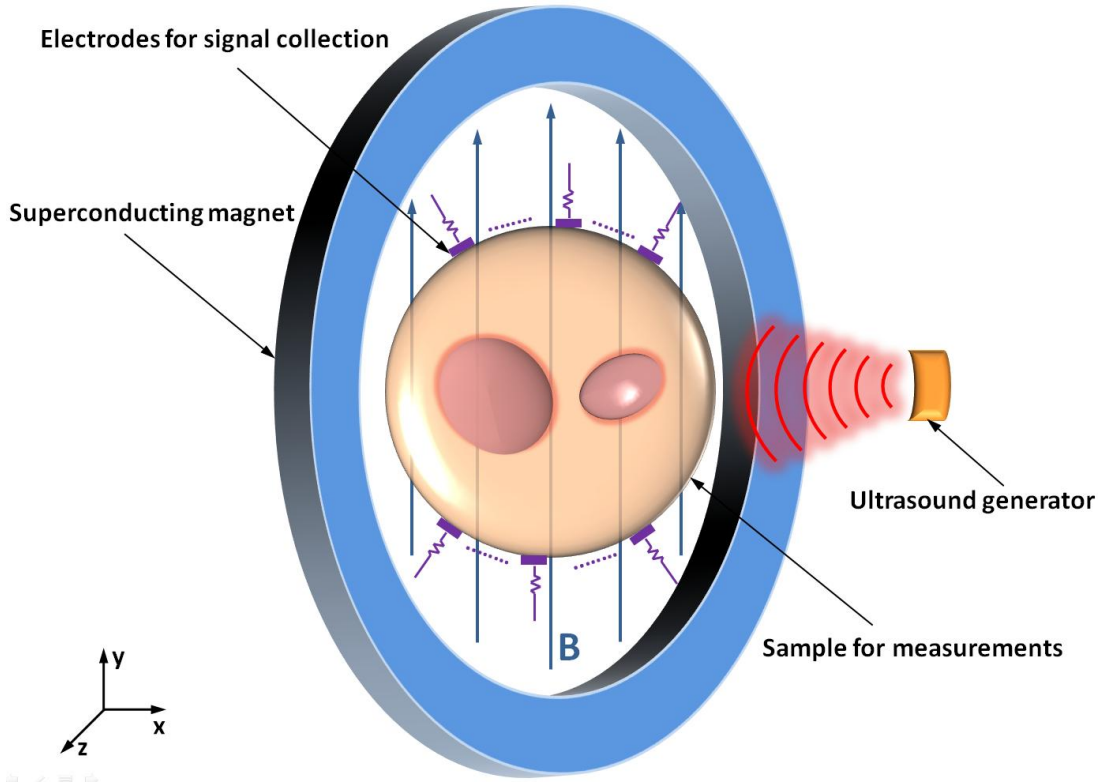

Fig. 1. Schematic of superconducting Lorentz Force Electrical Impedance Tomography (LFEIT).

Electrical Impedance Tomography (LFEIT). LFEIT is on the basis of electrical signal measurements arising when an ultrasound wave propagates through a conductive medium, which is vertically subjected to a magnetic field [1]. The magnitude of electrical signal is proportional to the strength of the magnetic field and the pressure of ultrasound wave [1].

In the 1990s, Hall Effect imaging (HEI) was developed by [3]. HEI use the Lorentz Force based coupling mechanism with ultrasound. HEI technology detects the Hall voltages using surface electrodes on the tested specimen, where these voltages are induced by using ultrasound to cause localised mechanical vibrations in a conductive tissue specimen located in a static magnetic field [3]. The spatial imaging of HEI is very close to ultrasound imaging, which is mainly determined by the bandwidth and central frequency of the ultrasound packets generated [1, 3]. The method of Magneto-acoustic tomography with magnetic induction (MAT-MI) was proposed by Bin He and his group, which has made the breakthrough to solve the shielding effect problem existed in other hybrid bio-conductivity imaging techniques [2]. Unlike HEI, MAT-MI use Lorentz force to induce eddy current to produce ultrasound vibrations which can be detected by using ultrasound transducers (receiving mode) placed around the specimen. Then, the recorded ultrasound signals are utilised to reconstruct the conductivity distribution of the biological sample [2, 6]. In 2013, a experimental Lorentz Force Electrical Impedance Tomography (LFEIT) was developed by Grasland-Mongrain et al [1]. Two specimen were chosen: a gelatin phantom and a beef sample, which were successively fixed into a 0.3 T magnetic field B_0 and sonicated with an ultrasonic transducer emitting 500 kHz bursts [1]. The results reveal that LFEIT has the potential to reach the spatial resolution of the ultrasound, and realize the detection of small inhomogeneities of soft tissue such as tumorous tissues.

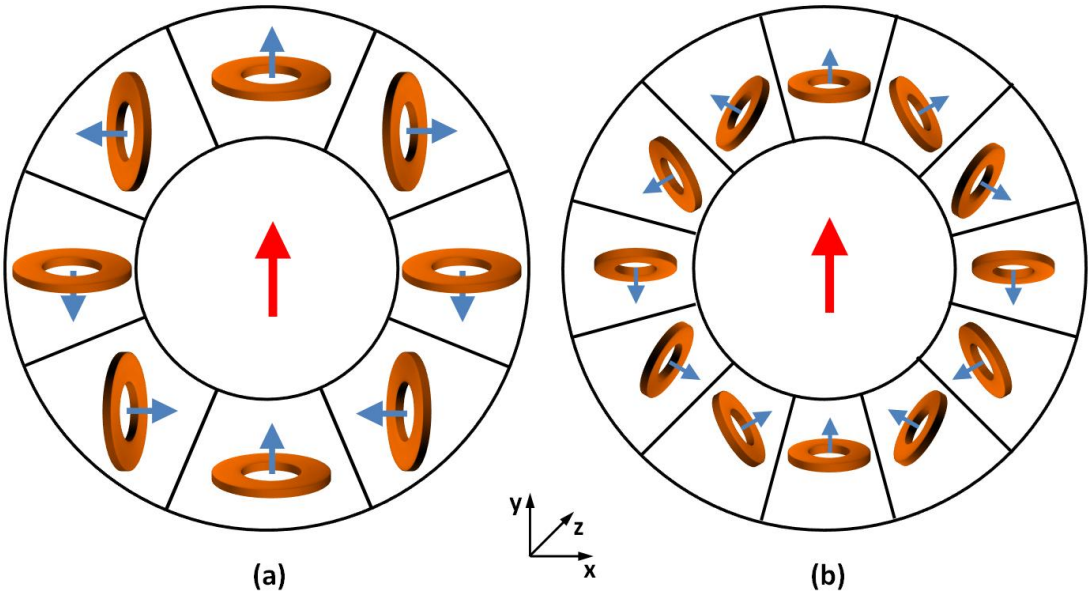

Fig. 2. Superconducting Halbach Array electromagnet: (a) 8 HTS coils, (b) 12 HTS coils.

As the magnetic field is crucial for generating the final electrical signal of LFEIT, authors have tried a novel combination of superconducting magnet with LFEIT system. The reason is that superconducting magnets can generate magnetic field with high intensity and homogeneity [7], which could efficiently enhance the electrical signal induced from sample thus improve the sound-to-noise ratio (SNR), particularly for a large scale full-body LFEIT. To the best of our knowledge, currently there is no research on design of LFEIT equipped with superconducting magnet. This paper presents the simulation of superconducting LFEIT system, which include the modeling of superconducting magnet using the FEM software COMSOL Multiphysics, coupled with the mathematical model of magneto-acoustic effect from LFEIT.

2. Modeling of superconducting magnet

The modeling of superconducting magnets was carried out on the basis of our previous work [8]. As the superconducting Helmholtz Pair, the conventional magnet structure for MRI, occupies a large space due to specific arrangement for Helmholtz coils location, the portability of LFEIT like equipping into general ambulances is difficult to realize [8]. Therefore, authors proposed superconducting magnets with thin geometry using the Halbach Array configuration [8, 9]. Superconducting coils were used to build an electromagnet operating below its critical temperature, which was able to generate a proper homogenous magnetic field. Fig. 2 presents the concept of superconducting Halbach Array magnet for 8 coils (each coil has 90 degree phase change) and 12 coils (each coil has 60 degree phase change).

COMSOL Multiphysics was chosen as the platform for the modeling of superconducting magnet, which was based on Partial Differential Equation (PDE) model with 2D ***H***-formulation. The general form of ***H***-formulation is [10]:

$$\mu_0 \mu_r \frac{\partial H}{\partial t} + \nabla \times \left(\rho \nabla \times H \right) = 0 \tag{1}$$

Where H is the magnetic field intensity, μ_0 is the permeability of free space, μ_r is the relative permeability, ρ is the resistivity. Here, ***B***-dependent critical current density and bulk approximation were also coupled into the modeling of superconducting magnet [11]:

$$J_c(B) = \frac{J_0}{\left(1 + \sqrt{\frac{k^2 {B_{para}}^2 + {B_{perp}}^2}{B_0}} \right)} \tag{2}$$

$$NI_t = \int J_t dA \tag{3}$$

Where J is the current density, B is the magnetic flux density. Equation (2) reveals J_c is reduced in the perpendicular and parallel magnetic field. J_0 is the critical current at 77 K within zero magnetic field. The parameters used in Equation (2) are $B_0 = 0.426$ and $k = 0.186$ presented in literature. In the magnet design, multiple tapes with layers of coated conductor were represented by continuous area bulk approximation to improve model simulation speed. Equation (3) indicates the multiplication of the transport current I_t in each tape and the number of turns N is identical to the integration of current density J_t inside bulk approximation with cross-section area A.

The 1.2 cm YBCO tape manufactured by SuperPower®, with critical 300 A at 77 K, was simulated as the coil material for superconducting Halbach Array. Fig. 3 presents the mesh for superconducting Halbach Array designs with (a) 8 HTS coils and (b) 12 HTS coils. Stacks of coils are represented by bulk approximation, and each pair bulk cross-sections represent 2000 turns (4×500 turns of a single layer rectangular coil) YBCO coils. As shown in Fig. 3, air was set in the ring centre and coils were fixed by the non-magnetic Halbach Array frame. A DC current 120 A was applied to each coil. Without changing the total amount of superconductor, Halbach Array configuration can use different numbers of coils, which can be realised by shrinking each coil's size with increasing number of coils (from 8 coils to 12 coils). The specification for these two superconducting Halbach Array designs is demonstrated in Table 1.

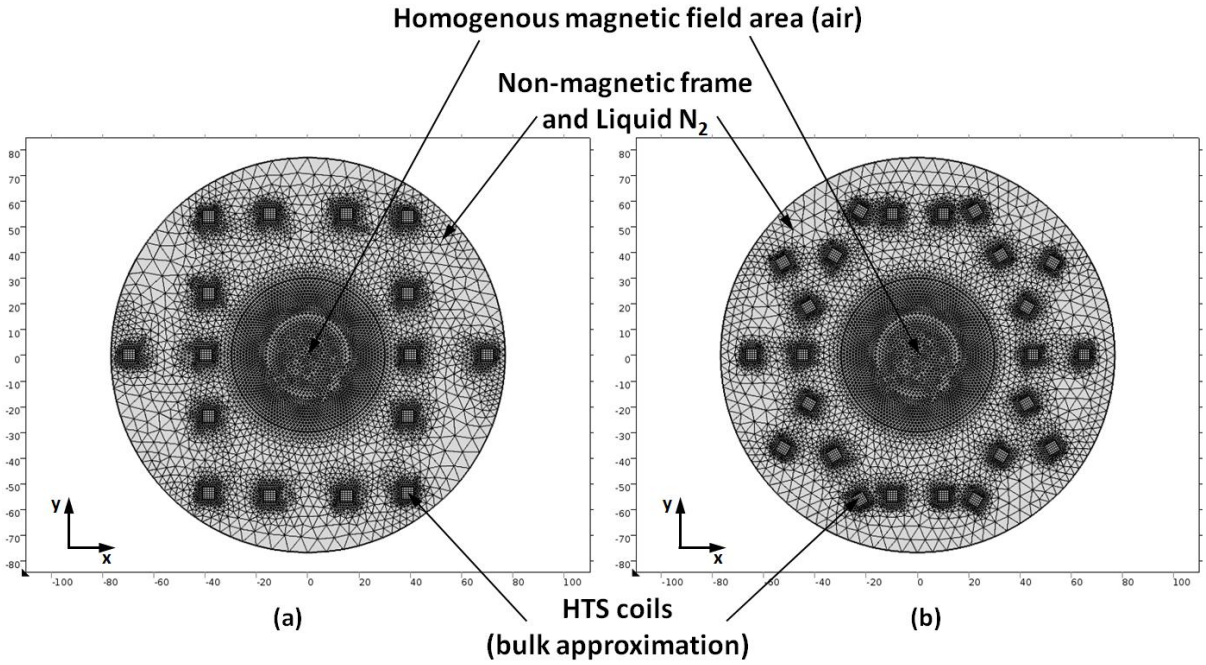

Fig. 3. Mesh for superconducting Halbach Array designs: (a) 8 HTS coils, (b) 12 HTS coils.

Parameters	Value
Inner diameter	60 cm
Outer diameter	156 cm
D_c (distance from coils centre to ring centre)	55 cm
μ_0	$4\pi\times10^{-7}$ H/m
n (E-J Power Law factor)	21
J_{c0}	10^8 A/m^2
E_0	10^{-4} V/m
I_{app}	120 A

Table 1. Specification for superconducting Halbach Array designs.

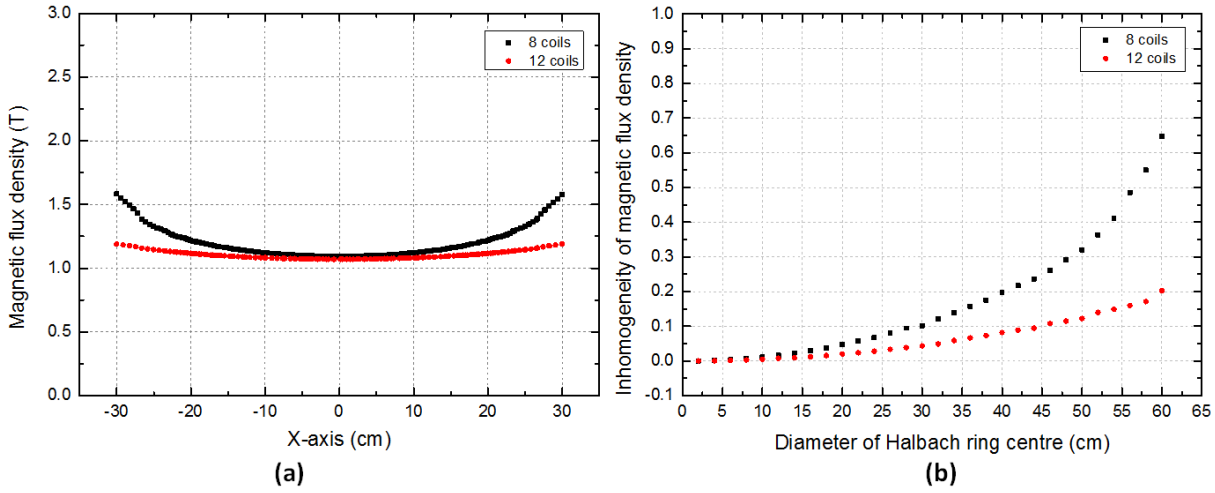

Fig. 4. (a) Magnetic flux density on diameter along x-axis of superconducting Halbach Array designs, with 8 coils and 12 coils, (b) Surface inhomogeneity of magnetic flux density in the Halbach ring centre cross-section with 8 coils and 12 coils configurations.

Fig. 4 (a) presents the magnetic flux density on diameter along x-axis of superconducting Halbach Array designs, with 8 coils and 12 coils. It can be discovered that the magnetic field becomes more homogenous when the coil's number increases from 8 to 12, and the magnetic flux density is all above 1 T for both cases. Precisely, Fig. 4 (b) presents the surface inhomogeneity of magnetic flux density in the cross-section of Halbach ring centre with 8-coils and 12 coils. With the increasing number of coils, the magnetic inhomogeneity has decreased significantly. For the 8 coils case, the inhomogeneity is approximately 30% (300 ppk: parts per thousand) within the circular region: 48 cm diameter of the centre cross-section. With the 12 coils case, the inhomogeneity is slightly over 10% (100 ppk) in the same circular region of 48 cm diameter. These magnetic properties were imported into the later mathematical model of LFEIT model.

3. Modeling of superconducting LFEIT system

3.1 Modeling of acoustic module

Acoustic module was to generate ultrasound waves to causes localised mechanical vibrations in a conductive tissue located in a static magnetic field, from which these Hall voltages are induced.

Fig. 5 demonstrates the Simulation of ultrasound pressure field which was based on the ultrasound MATLAB package from FOCUS [12]. This acoustic module used ultrasound phase array structure, which consisted of 32 transducer elements with each generating 1 MHz ultrasound signal. The focused region had 1 mm width and 10 cm length, and the focused ultrasound pressure was approximately at 3 MPa. The location of the ultrasound focused

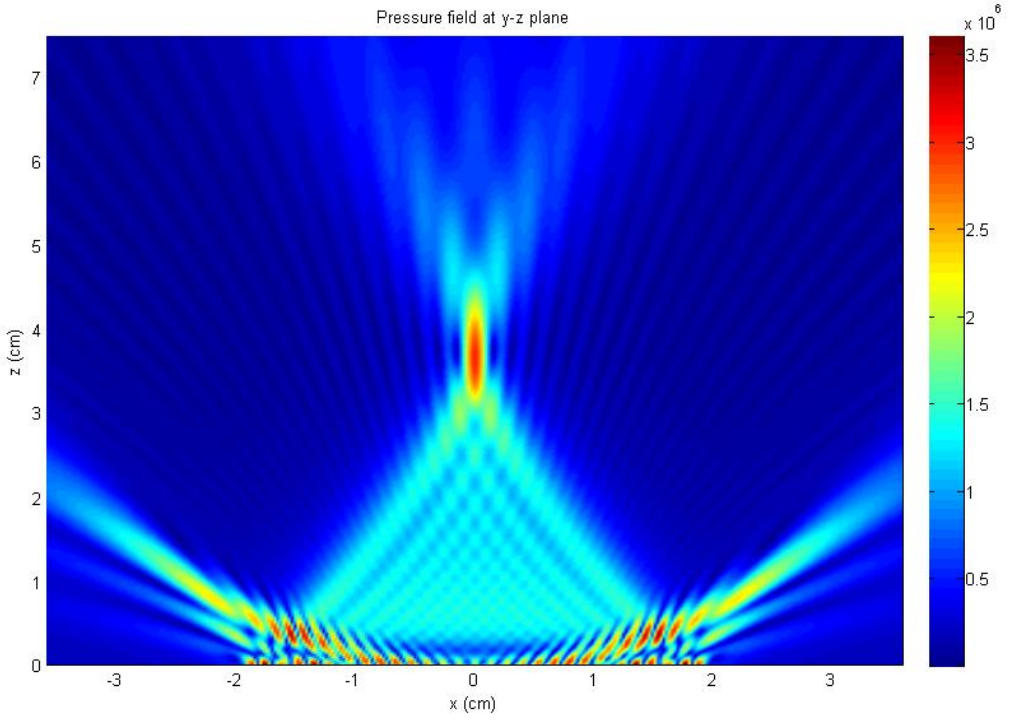

Fig. 5. Simulation of ultrasound pressure field.

point could be tuned by changing the phase delay of each transducer. The speed of ultrasound was set as the average value 1500 m/s in human tissues [12]. The attenuation coefficient was set as 8×10^{-2} dB/cm/MHz which is close to the value for human muscle [12].

3.2 Modeling of electrical signal

This section describes the mathematical model of LEFIT system. According to the formula of Lorentz force [13]:

$$F = qv \times B \tag{4}$$

Where q is charge of particle move with velocity v, and $\boldsymbol{B}$ is magnetic flux density. This Lorentz force is also equivalent to the force caused by the induced electric field [13]:

$$F = qE \tag{5}$$

Meanwhile, the relation of electrical conductivity is [13]:

$$J = \sigma E \tag{6}$$

Combining Equation (4), (5) and (6), the equation for transient current density can be derived:

$$J = \sigma v \times B \tag{7}$$

Assuming the ultrasound wave propagating along z direction, the ultrasound bean width is W and ultrasound path is L, the voltage measurement can be described as [3]:

$$V_h(t) = \alpha R W B_0 \int_L \sigma(z) v(z,t) dx \tag{8}$$

Where α is a percentage constant representing the efficiency current collected by the electrodes, B_0 is the static magnetic field and R is the total impedance of measurement circuit. According the formula for relation of sound pressure and particle movement velocity [14], z direction term can be:

$$v_z = -\frac{1}{\rho_0} \int \frac{\partial p}{\partial z} dt \tag{9}$$

The ultrasound momentum M can be expressed by using the time integration of ultrasound pressure with regard to time τ [3, 14]:

$$M(z,t) = \int_{-\infty}^{t} p(z,\tau) d\tau \tag{10}$$

Therefore, that the governing equation for final output signal of LFEIT can be determined by combining Equation (8), (9) and (10) [3]:

$$V_h(t) = \alpha RWB_0 \int_L M(z,t) \frac{\partial}{\partial z} \left[\frac{\sigma(z)}{\rho(z)} \right] dx \tag{11}$$

Equation (11) reveals that magnitude of final output signal is proportional to the strength of magnetic field and the ultrasound pressure. More importantly, output signal is nonzero only at the interface where the gradient of electrical conductivity over mass density $\nabla(\sigma/\rho)$ is not zero. The mathematical MATLAB model of LFEIT system was built based on governing equations (11).

For this model, it is assumed on the basis of literature [1, 15] that the gradient of electrical conductivity over mass density of two interfaces is in second-order form:

$$\frac{\partial}{\partial z}(\sigma / \rho) = a\left(c - (z-b)^2\right) \tag{12}$$

The sample shown in Fig. 6 was simulated as a human tissue which was immersed into the oil. This sample had a round shape cross-section whose diameter was 8 cm, and it located in absolute uniform magnetic field 1 T with zero noise. The gradient of electrical conductivity over mass density of two interfaces $\nabla(\sigma/\rho)$ was set as: a = 0.03, b = 6 and c = 36 for Equation (12). It can be seen from Fig. 6 that the absolute value of output signal matches the overshot of a second-order form. The ideal output signal level is in 1 μV order and peak quantity is around 2.5 μV according to the simulation.

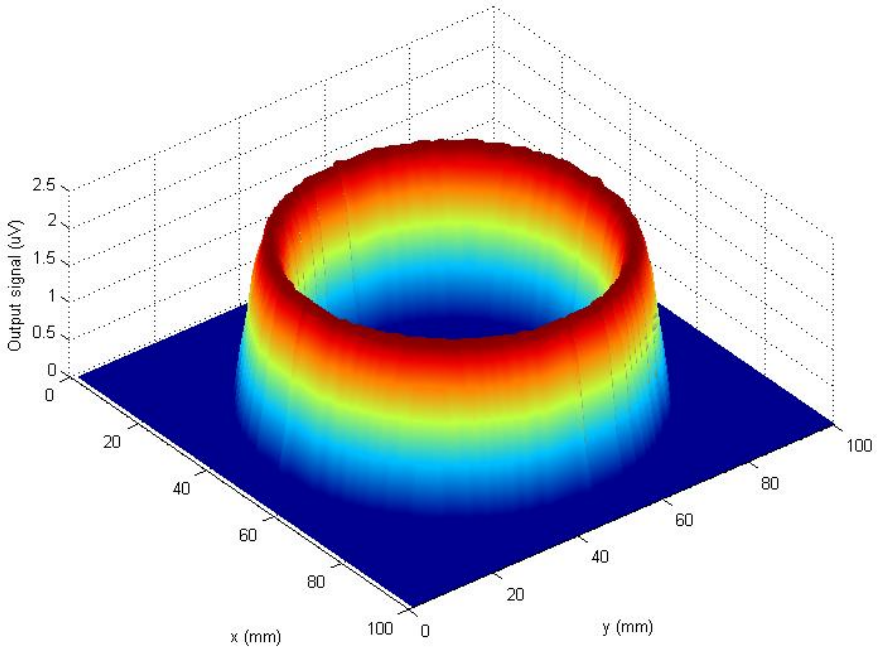

Fig. 6. Ideal output signal (absolute value) detected from sample with absolute uniform magnetic field 1 T and zero noise.

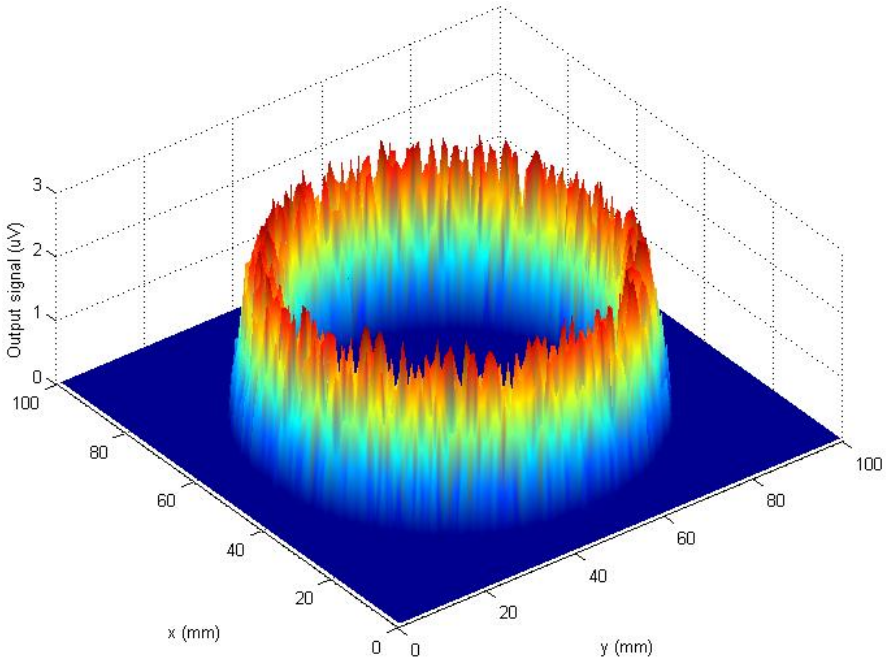

Fig. 7. Output signal (absolute value) detected from sample located in magnetic field with 30% inhomogeneity.

Output signal will be distorted if the magnetic field in the testing area has 30% inhomogeneity, which is shown in Fig. 7. Based on the literatures [3], the noise signal level for LFEIT or HEI experiment is around 1 μV for 1 MHz input ultrasound signal. Thus a white Gaussian noise with rms value 1.5 μV was added into the entire testing region of this model, which is presented in Fig. 8.

3.3 Imaging of electrical signal and comparison

After obtaining the electrical signal distribution of the biological sample's cross-section, the fundamental method for imaging can be used to determine the location and external shape of

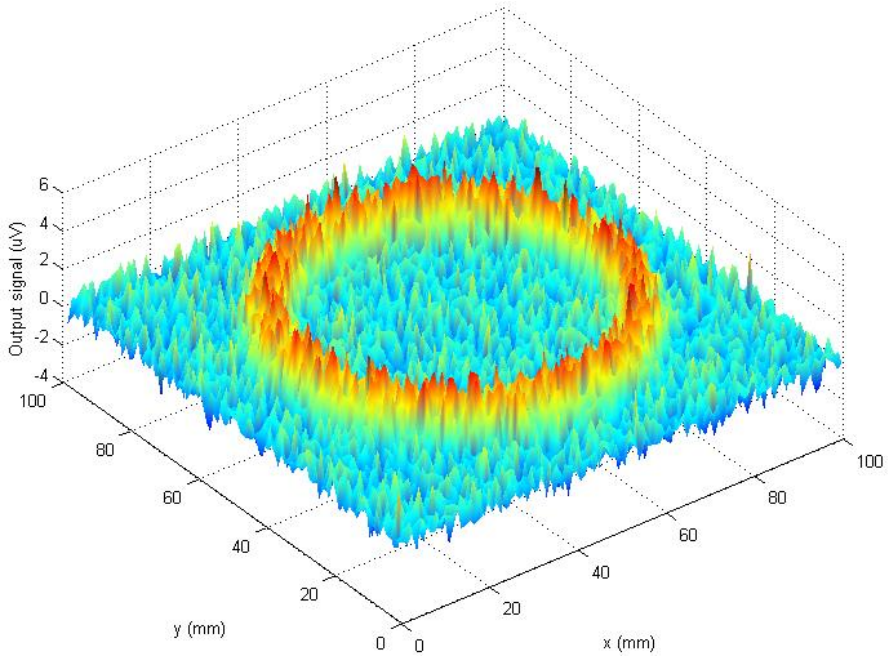

Fig. 8. Output signal detected from sample located in 30% inhomogeneity magnetic field with noise condition.

biological sample, as electrical signal can only be induced at the different interface within the sample due to the LFEIT's physical principle. The basic imaging method with the "imshow" command of MATLAB was used to map the electrical signals. There were two biological samples for simulation, and both of them were assumed to be fully immersed into oil. The first sample had the gradient of electrical conductivity over mass density $\nabla(\sigma/\rho)$ of Equation (12) with coefficient $a = 0.03$, $b = 5$ and $c = 25$, and the second sample had the $\nabla(\sigma/\rho)$ of Equation (12) with coefficient $a = 0.1$, $b = 2$ and $c = 4$. Similarly, the entire testing region was simulated with a white Gaussian noise whose rms value was 1.5 μV, and the source of ultrasound was assumed to be unchanged. The magnetic field properties from magnet designs were imported into the LFEIT model. Fig. 9-11 present the simulation for these two samples tested by LFEIT system, with different magnetic field strength and uniformity.

Fig.9 illustrates voltage output and the electrical signal imaging from the samples located in the 0.5 T magnetic field with 30% inhomogeneity (using the 8-coil magnet with 60 A current, and using the field area near the edge of circular region d=50 cm). It can be discovered from Fig. 9 (a) that both of the voltage outputs (absolute value) were distorted due to the inhomogeneity of magnetic field. Fig. 9 (b) presents output signals were almost submerged by the noise because the magnitude of voltage outputs was declined after distortion, and the output signals from second sample were almost blow than 1.5 μV. The average SNR was only 3.6 dB. The image reconstruction of electrical signal is faint and it is very difficult to find the edge and location of second sample.

In contrast with Fig. 9, Fig. 10 presents a magnetic field with higher uniformity (10% inhomogeneity) which was applied into LFEIT system, but the strength of magnetic field still maintained the same (using the 12-coil magnet with 60 A current, and using the field area near the edge of circular region d=50 cm). Compared with Fig. 9 (a), it can be found that both of the voltage outputs (absolute value) has less distorted due to the better uniformity of magnetic field. As shown in Fig. 10 (b), although the average SNR improved to 5.6 dB, most output signals from second sample were still missing after adding the noise. The quality of electrical signal imaging from Fig. 10 is slightly better than that of Fig. 9, and the boundary of second sample can be hazily seen from Fig. 10 (c).

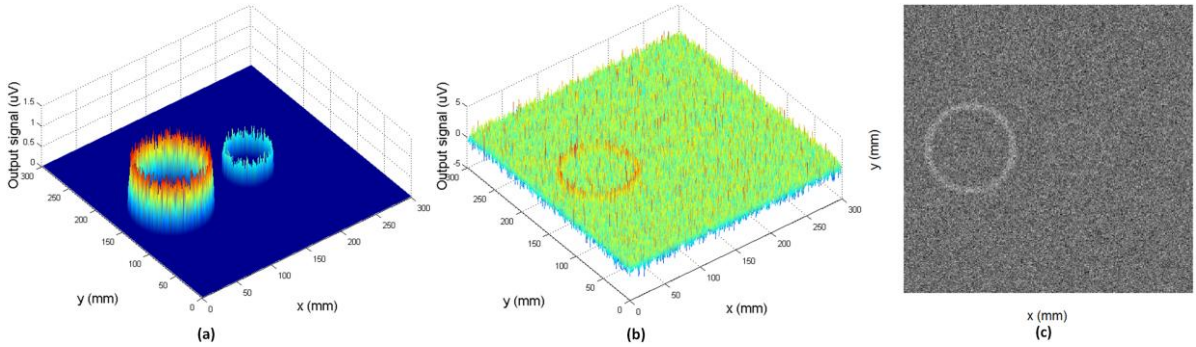

Fig. 9. (a) Voltage output (absolute value) without noise, (b) with noise, (c) electrical signal imaging, from the sample located in the 0.5 T magnetic field with 30% inhomogeneity.

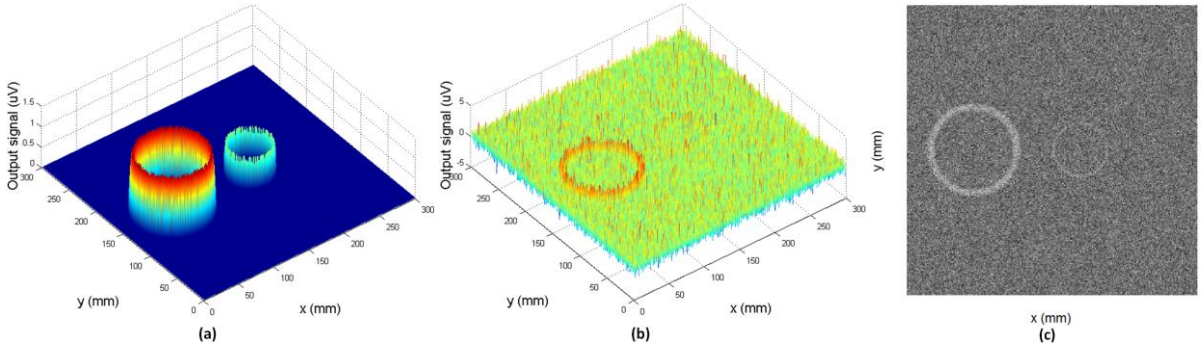

Fig. 10. (a) Voltage output (absolute value) without noise, (b) with noise, (c) electrical signal imaging, from the sample located in the 0.5 T magnetic field with 30% inhomogeneity.

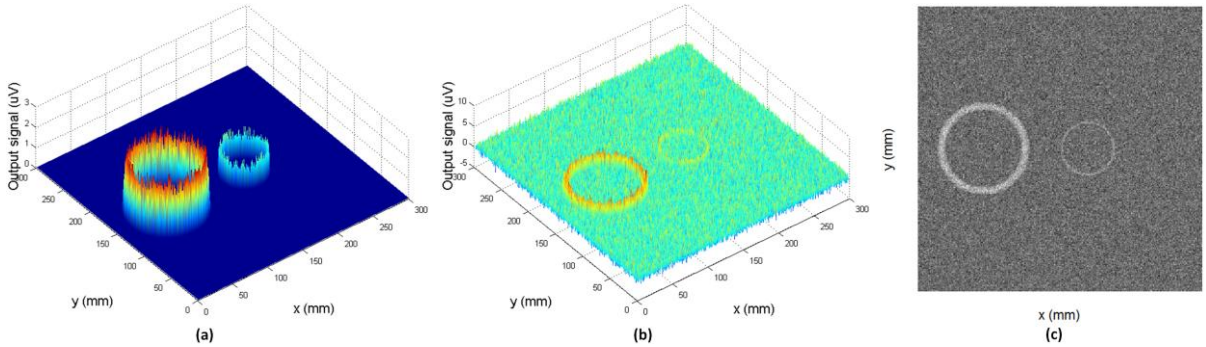

Fig. 11. (a) Voltage output (absolute value) without noise, (b) with noise, (c) electrical signal imaging, from the sample located in the 1 T magnetic field with 30% inhomogeneity.

Fig. 11 demonstrates the simulation of output signals and the electrical signal imaging where the sample was tested in the 1 T magnetic field with 30% inhomogeneity (using the 8-coil magnet with 120 A current, and using the field area near the edge of circular region d=50 cm). The strength of magnetic field was doubled compared with previous two simulations. It can be seen from Fig. 11 (b) that most voltage outputs from both samples were greater than the average noise level (average SNR 11.8 dB), although voltage outputs were distorted by 30% inhomogeneity of applied magnetic field. As the result, the imaging of electrical signals from Fig. 11 (c) is much clearer than that from Fig. 9 (c) and Fig. 10 (c), and the edge and shape of both samples can be discovered.

3.4 Summary

To summarise, both increasing the magnetic field strength and improving the uniformity of magnetic field can improve quality of electrical signal imaging of LFEIT. However, increasing the intensity of magnetic field is more effective, especially when the noise level is comparable with the electrical signal generated from sample. Imaging quality of electrical signal was still acceptable when more than 10% inhomogeneity of static magnetic field was applied LFEIT system with magnetic flux density around 1 T. The tolerance of magnetic field inhomogeneity for LFEIT system is several orders high than that of MRI, due to LFEIT shares the characteristic of ultrasound imaging [1]. The design above simulated and imaged the electrical signals generated by LFEIT, which could be used to find the approximate location and the boundary shape of a certain tissue. Nevertheless, for detail imaging of impedance distribution, future works are required to be carried out.

4. Conclusion

The modeling of superconducting Halbach Array magnets were executed using COMSOL Multiphysics as the FEM platform, which was on the basis of Partial Differential Equation model with 2D $\boldsymbol{H}$-formulation coupling $\boldsymbol{B}$-dependent critical current density. Without altering the total amount of superconductor, simulation results indicate homogeneity of magnetic field has been remarkably improved by shrinking each coil's size while increasing the coils' number for Halbach configuration (from 8 coils to 12 coils). The mathematical model for LFEIT system was constructed, which was based on magneto-acoustic effect together with the magnetic properties from magnet design. Two samples located in three different magnetic fields are simulated by the LFEIT model. According to the simulation results, both uniformity and strength of magnetic field affected electrical signal from LFEIT. By contrast, increasing magnetic intensity is more efficient, particularly if the bio-induced electrical signal is lower than or comparable with the noise level. The performance of signal imaging is still acceptable when more than 10% inhomogeneity of magnetic flux density (around 1 T) is applied LFEIT system. The combination of superconducting magnet with LFEIT system is a reasonable approach because superconducting magnets are able to produce magnetic field with high intensity and good homogeneity, which could potentially enhance the SNR of LFEIT system and the quality of biological imaging.

Acknowledgments

This work was carried out with the help of the Electrical Engineering Division, Department of Engineering, University of Cambridge. Authors would like to express gratitude to all the members of staff there for their important assistance. Some of the authors are research students, and they are grateful to China Scholarship Council (CSC) for their scholarships and support for overseas study.

References

[1] P. Grasland-Mongrain, J. Mari, J. Chapelon, C. Lafon, Lorentz force electrical impedance tomography, IRBM, 34 (2013) 357-360.

[2] Y. Xu, B. He, Magnetoacoustic tomography with magnetic induction (MAT-MI), Physics in medicine and biology, 50 (2005) 5175.
[3] H. Wen, J. Shah, R.S. Balaban, Hall effect imaging, Biomedical Engineering, IEEE Transactions on, 45 (1998) 119-124.
[4] C. Gabriel, S. Gabriel, E. Corthout, The dielectric properties of biological tissues: I. Literature survey, Physics in medicine and biology, 41 (1996) 2231.
[5] H. Schwan, K. Foster, RF-field interactions with biological systems: electrical properties and biophysical mechanisms, Proceedings of the IEEE, 68 (1980) 104-113.
[6] L. Mariappan, B. He, Magnetoacoustic tomography with magnetic induction: Bioimepedance reconstruction through vector source imaging, Medical Imaging, IEEE Transactions on, 32 (2013) 619-627.
[7] T. Coombs, Z. Hong, Y. Yan, C. Rawlings, The next generation of superconducting permanent magnets: The flux pumping method, IEEE Trans. Appl. Supercond., 19 (2009) 2169-2173.
[8] B. Shen, L. Fu, J. Geng, H. Zhang, X. Zhang, Z. Zhong, Z. Huang, T. Coombs, Design of a Superconducting Magnet for Lorentz Force Electrical Impedance Tomography, IEEE Transactions on Applied Superconductivity, 26 (2016).
[9] K. Halbach, Design of permanent multipole magnets with oriented rare earth cobalt material, Nucl. Instrum. Methods., 169 (1980) 1-10.
[10] Z. Hong, A. Campbell, T. Coombs, Numerical solution of critical state in superconductivity by finite element software, Superconductor Science and Technology, 19 (2006) 1246.
[11] M. Ainslie, Y. Jiang, W. Xian, Z. Hong, W. Yuan, R. Pei, T. Flack, T. Coombs, Numerical analysis and finite element modelling of an HTS synchronous motor, Physica C: Superconductivity, 470 (2010) 1752-1755.
[12] R. McGough, FOCUS, in, Michigan State University, 2015.
[13] M.A. Salam, Electromagnetic field theories for engineering, Springer Science & Business Media, 2014.
[14] H. Azhari, Basics of biomedical ultrasound for engineers, John Wiley & Sons, 2010.
[15] T. Heida, W. Rutten, E. Marani, Understanding dielectrophoretic trapping of neuronal cells: modelling electric field, electrode-liquid interface and fluid flow, Journal of Physics D: Applied Physics, 35 (2002) 1592.